Saudi Pharmaceutical Journal 28 (2020) 349–361

Contents lists available at ScienceDirect

Saudi Pharmaceutical Journal

journal homepage: www.sciencedirect.com

Original article

Formulation and evaluation of cyclodextrin-based nanosponges of griseofulvin as pediatric oral liquid dosage form for enhancing bioavailability and masking bitter taste

Samia M. Omar [a,b,*], Fares Ibrahim [a], Aliaa Ismail [a]

[a] Department of Pharmaceutics, Faculty of Pharmacy, Helwan University, Egypt
[b] Department of Pharmaceutics, Faculty of Pharmacy, Ahram Canadian University, Egypt

ARTICLE INFO

Article history:
Received 21 October 2019
Accepted 29 January 2020
Available online 3 February 2020

Keywords:
Griseofulvin
Nanosponges
Cyclodextrin
Taste masking
Bioavailability

ABSTRACT

The aim of this study was the development of griseofulvin (GRI) loaded β-cyclodextrin (β–CD) based nanosponges for bitter taste masking, improving dissolution rate and oral bioavailability. Plain NS (NS1 NS2 and NS3) were fabricated by reacting β-CD with the cross-linker diphenyl carbonate at different molar ratios (1:2, 1:4 and 1:6, respectively) using ultrasonication method. The NS2 provided both highest %yield and GRI solubilization enhancement. Thus, the drug was loaded in NS2 at different NS2: drug weight ratios in presence or absence of 0.25%w/w polyvinylpyrolidone (PVP k30). The GRI loaded NS (F1) that provided highest drug loading capacity and entrapment efficiency (47.20 ± 0.38%, 84.91 ± 0.30%, respectively) was morphologically examined using scanning electron microscopy (SEM). Also, Particle size, zeta potential, differential scanning calorimetry (DSC), Fourier transform infra-red (FT-IR), nuclear magnetic resonance (NMR) spectroscopy, *in-vitro* release, taste masking potential were evaluated. Moreover, *in-vivo* Pharmacokinetic studies were performed on rats. The F1 showed particle size 665.9 ± 13.8 nm and zeta potential −21.5 ± 0.7 mV. The DSC and FT-IR analysis confirmed the complexation of GRI with NS2. Nanosponges (F1) provided 3.19, folds increase in dissolution efficiency %, 2.13 and 3.78 folds increase in C_{max} and AUC_{0-48} compared to plain GRI. Taste masking evaluation confirmed the potential of GRI nanosponges (F1) in masking the bitter taste of GRI completely. The study confirmed that complexation of GRI with NS would be a viable approach for masking the bitter taste of GRI and improving oral bioavailability, that Cmax, Tmax and AUC 0–48 were significantly higher for the developed formulation (F1).

1. Introduction

Griseofulvin (GRI) is an antifungal agent derived from the mold *Penicillium griseofulvum* (Dash and Mishra, 2012). It is administered orally for the treatment of dermatophyte and ringworm infections. It is generally given for infections that involve the scalp, hair, nails and skin which do not respond to topical treatments (Castiglione et al., 2013). Griseofulvin has long been approved by FDA as the agent of choice for treatment of tinea capitis in children. It has an established efficacy and safety profile, and it is relatively inexpensive (Bennett et al., 2000).

Solubility of GRI in water is 8.64 mg/L and log P (octanol/water) is 2.15 (Arida et al., 2007). According to Biopharmaceutics Classification System (BCS), GRI belongs to class II drugs for which the dissolution rate is the primary limiting aspect to the absorption (Amidon et al., 1995). Moreover, bitter taste is one of the potential problems associated with this drug. For pediatric patients, liquid formulations are usually recommended as they are easy to be administered. However, the production of such formulations may be limited by the drug solubility.

There were various formulation approaches used for GRI solubility enhancement, like micronization by supercritical fluid technology (Reverchon et al. 2004), solid dispersion (Chiang et al., 2013), self-emulsifying drug delivery system (Arida et al., 2007), nanocrystallization (Dandagi et al., 2011). polymeric micelles

* Corresponding author at: Department of Pharmaceutics, Faculty of Pharmacy, Helwan University, Egypt.
E-mail address: omarsamia3@hotmail.com (S.M. Omar).

Peer review under responsibility of King Saud University.

Production and hosting by Elsevier

https://doi.org/10.1016/j.jsps.2020.01.016
1319-0164/

(Sharifmakhmalzadeh, Khodarahmpour, & Salimi, 2014). Also, inclusion complexation with β-cyclodextrin was adapted (Dhanaraju et al., 1998).

Cyclodextrins are very useful in the pharmaceutical industry as they can increase the solubility of drugs and mask some of the organoleptic characteristics leading to an improved compliance (Ahuja et al., 2011). However, the use of native cyclodextrins for the preparation of inclusion complexes suffers from limitations, as the ease of separation of the complex upon dilution, and size requirements of the drug molecules which exclude complexation of molecules having high molecular weight or aqueous solubility. Moreover, cyclodextrins suffer from limited aqueous solubility as a result of the strong intermolecular hydrogen bonding in the crystal state (Cavalli et al., 2006).

Recently, in order to enhance the inclusion capacity of native cyclodextrins, the synthesis of cyclodextrin based nanosponges has emerged as a trend in cyclodextrin-based drug delivery and usually reported to enhance the encapsulation ability (Ansari et al., 2011; Nash, 2002; Zoppi et al., 2008). Nanosponges are obtained by reacting cyclodextrins with a cross-linking agent like carbonyldiimidazole, dimethyl carbonate, diphenyl carbonate (Cavalli et al., 2006). Nanosponges are generally developed using β-cyclodextrin because of its low cost and the high complexing extent along with stability with the crosslinking agents as compared to other types of cyclodextrins (Ansari et al., 2011). Cyclodextrin based nanosponges are generally developed by either a melt procedure, solvent method or ultrasonication technique (Ansari et al., 2011; Cavalli et al., 2006; Trotta et al., 2008).

Nanosponges are formed as three-dimensional networks of spherical porous particles having colloidal sizes with a mean diameter of less than 1 μm and narrow size distribution and form opalescent suspensions when dispersed in water (Cavalli et al., 2006; Trotta et al., 2012). Cyclodextrin - based nanosponges are able to form inclusion and non-inclusion complexes with drug molecules due to both their existing native cyclodextrins cavities and nano-porous network structure (Cavalli et al., 2006; Moya-Ortega et al., 2012; Tejashri et al., 2013; Trotta et al., 2012). Nanosponges are considered to be one of the most promising nanosized delivery system because of its high stability, high carrier capacity and feasibility of incorporation of both hydrophilic and hydrophobic substances. Moreover, nanosponges can improve the solubility, chemical stability and, consequently, the bioavailability of lipophilic drugs (Cavalli et al., 2006). It was reported that cyclodextrin-based nanosponges was successfully developed as a carrier for gapabentin with taste masking potential (Rao and Bhingole, 2015).

The objective of the study was the development of GRI loaded NS and evaluation of their physicochemical properties and *in-vivo* absorption aiming in enhancing the dissolution and bioavailability of GRI with masking its bitter taste.

2. Experimental

2.1. Materials

Griseofulvin (GRI), β -Cyclodextrin (β-CD) and Diphenyl Carbonate (DPC) were purchased from Sigma Al-drich (St. Louis, USA). Poly vinyl pyrolidone K30 was obtained from Acros Organics (Belgium). Ferric Chloride was obtained from Alpha Chemika (Mumbai, India). Ethanol (LC-MS grade), Acetonitrile, Formic acid, Methanol and Propranolol hydrochloride were purchased from Sigma Aldrich (Chemie GmbH, Steinheim, Germany). Ultra-pure grade water used throughout the study was prepared from deionized water, PURELAB Prima, VWS Ltd. (ELGA- Lab Water Global Operation Centre, High Wycombe, HP14 3BY, Bucks, UK). All other chemicals and solvents were commercially available analytical grade materials.

3. Methodology

3.1. Preparation of plain beta cyclodextrin nanosponges (β-CD NS)

Different plain β-CD NS (NS1, NS2 and NS3) were prepared via ultrasonication assisted cross-linking reaction of β-CD using diphenyl carbonate (DPC) as cross-linker (ultrasound assisted method) (Trotta et al., 2008). Briefly, anhydrous β-CD (molecular weight 1135 g/mol) and DPC (molecular weight 214.216 g/mol), finely homogenized by trituration, were placed in a 250 ml conical flask. The mixture was gradually heated to 100 °C using water bath ultrasonic (ELMA Schmidbauer GmbH, Elmasonic S 30H, TYPE: S30H, IP: 20, Germany), and left to react for 5 hrs. During the reaction crystals of phenol appeared at the neck of the flask. The carbonyl functional group of DPC was responsible for cross-linking the β-CD molecules and resulting in liberation of phenol. The reaction mixture was left to cool then phenol crystals were carefully removed and the product was broken up roughly. The resulted solid was repeatedly washed with 50 ml distilled water to remove unreacted β-CD and then with 100 ml ethanol, to remove the unreacted DPC and phenol present as by-product of the reaction. After every washing, test for phenol was carried out by adding 2 drops of 1%w/v ferric chloride solution to washing water (Rao and Shirsath, 2017). The reaction was carried out at three different molar ratios, e.g. 1:2, 1:4, 1:6 (β-CD: DPC cross-linker) for NS1, NS2 and NS3, respectively. The product obtained was a fine white powder. The prepared blank NS were stored at room temperature until further use.

3.2. Percent yield of plain β-CD NS

The prepared plain nanosponges were weighed and the yield was calculated for each preparation using the following formula (Furniss, 1989):

$$\%\text{Yield} = \frac{\text{wtofNS}}{(\text{wtof}\beta - \text{CD} + \text{wtofDPC})} \times 100 \quad (1)$$

3.3. Construction of the GRI – β cyclodextrin as well as GRI-NS (NS2 and NS3) phase solubility diagrams

The solubility studies for GRI were performed according to the method previously described (Higuchi and Connors, 1965). Briefly, known excess weight of GRI (30 mg) was added to screw capped vials containing 10 ml aqueous solution of different molar concentrations of the β-cyclodextrins, 0 to 13.22 mM (saturation solubility of β-CD) (Dua et al., 2011), as well as, to 10 ml aqueous solution of different concentrations of NS2 and NS3 (0–2% w/v) (Swaminathan et al., 2007), The vials were allowed to be mechanically shaken in water bath shaker at 37 ± 0.5 °C. Hundred μL aliquots were withdrawn from vials, filtered with hydrophilic cellulose acetate sterile syringe filter (pore size 0.22 μm, diameter 25 mm). Then the clear filtrates were diluted appropriately with DMF and analyzed for GRI concentration using UV spectroscopy at λ_{291nm}. The sample withdrawal process was repeated every 24 hrs till equilibrium was reached.

The apparent stability constant (Kc) was calculated from the initial straight portion of the phase solubility diagram using the following equation (Higuchi and Connors, 1965):

$$kc = \frac{slope}{S_0(1 - slope)} \quad (2)$$

where Kc is the apparent stability constant, S_o is the inherent solubility of substrate and Slope is the slope of straight portion of the phase solubility diagram.

3.4. Molecular modeling studies for prediction of the best binding mode of griseofulvin by docking study

The possibility of complex formation and the binding mode of griseofulvin within the structure of β-cyclodextrin nanosponge was predicted by using molecular docking study (Rao and Bhingole, 2015; Rao et al., 2018). The structure of a unit of the polymer was built, prepared and the docking process was applied using Molecular Operating Environment (MOE®) version 2013.08 (Chemical Computing Group Inc., Montreal, QC, Canada). Resveratrol was used as a reference as it was reported previously to have good binding and applications in drug delivery system with β-cyclodextrin nanosponge (Ansari et al., 2011).

3.5. Preparation of GRI –loaded NS

Nanosopnges loaded with GRI were prepared at different weight ratios (1:1, 1:2, 1:3, 1:4) of the previously developed nanosponges (NS2) to the drug in presence or absence of 0.25%w/w polyvinyl pyrrolidone (PVP K30) (of total preparation weight). Eight formulae (F1- F8) were prepared as shown in Table 1. A method described previously for nanosponges drug loading was followed (Swaminathan et al., 2013). The drug was dispersed in aqueous colloidal dispersions of plain nanosponges with either 0%w/w or 0.25% w/w PVP. The suspensions were stirred for 24 hrs then centrifuged using a table top high speed refrigerated centrifuge (Bio Lion XC-HR20, Manassas, USA) at 2000 rpm for 10 min to separate the uncomplexed drug as a residue below the colloidal supernatant. The colloidal supernatants were freeze-dried (Christ Alpha 1–2 LD, Osterode am Harz, Germany) to obtain drug-loaded NS formulations. The drug-loaded NS formulations were stored at room temperature for further use.

3.6. Determination of percentage of drug loading in the prepared NS

The obtained freeze dried GRI loaded NS were weighed accurately and dissolved in appropriate volume of DMF. Drug content was analyzed using UV Spectrophotometer (Jasco, Japan). The percent drug loading capacity was calculated for each preparation using the following formula (Zainuddin et al., 2017).

$$\%\ \text{Drug loading} = \frac{\text{Actual drug content in (GRI} - \text{NS)formulation}}{\text{wt of(GRI} - \text{NS) formulation}} \times 100 \quad (3)$$

3.7. Characterization of the selected GRI loaded NS formula (F1)

3.7.1. Scanning electron microscopy examination (SEM)

The surface morphology of freeze dried GRI loaded NS formula (F1) was examined by scanning electron microscope (FE-SEM quanta FEG 250, Holland) using high vacuum mode. The samples were coated by gold sputter coater (SPI-Module). Digital images of the samples were obtained at an accelerating voltage of 20 kV.

Table 1
The prepared GRI loaded NS formulae.

FormulaNo	Plain NS2 : GRI (w/w)	PVP(0.25%w/w)
F1	1:1	*
F2	1:1	–
F3	1:2	*
F4	1:2	–
F5	1:3	*
F6	1:3	–
F7	1:4	*
F8	1:4	–

* PVP is included in the NS/GRI aqueous dispersions.

3.7.2. Determination of particle size, polydispersity index (PDI) and zeta potential

The mean particle size, polydispersity index (PDI) and zeta potential of the selected NS formula (F1) were determined using Malvern® Zetasizer (Worcestershire, UK). Each sample was diluted suitably with distilled water prior to measurements. All samples were measured at 25 ± 0.5 °C in triplicates and results were represented as mean value standard deviation (±SD).

3.7.3. Differential scanning calorimetry (DSC)

To confirm the interaction (if any) of GRI with any of the excipients added and withstand of the drug during the loading process of nanosponges, Scanning Calorimetry (DSC) studies were carried out for GRI, β-CD, PVP K30, plain NS2 and F1. The analysis was performed using Shimadzu DSC-50 instrument equipped with a computerized data station. Five mg samples were heated in a temperature range of $33 - 300^{\circ}C$ at rate of $10^{\circ}C$/min in flat-bottom aluminum pans in presence of nitrogen at flow rate of 30 ml/min. An empty aluminum pans were used as a reference.

3.7.4. Fourier transform infrared (FT-IR) spectroscopy

To study the interaction (if any) of GRI with any of the excipients added and the stability of the drug during the loading process of nanosponges, Fourier transform infrared (FT-IR) spectroscopic studies were carried out for GRI, β-CD, PVP K30, plain NS2 and F1. The analysis was performed using potassium bromide (KBr) disc method. Approximately 2–3 mg samples were carefully mixed with KBr, palletized under vacuum and then analyzed using FT-IR spectrophotometer (Genesis II FT-IR, Mattson, USA) at range of 4000–400 cm^{-1}

3.7.5. Nuclear magnetic resonance (NMR) spectroscopy

Determination of the 1H NMR spectra of NS-GRI (F1) was done using a Bruker Avance 400 MHz spectrometer, with 16 scans. Stock solutions of the NS, GRI and F1 were prepared in deuterated DMSO. Deuterated DMSO was chosen as solvent since the NS is not soluble in deuterated water/chloroform, and previous studies have shown that DMSO does not interfere in the formation of the inclusion compounds (Silva et al., 2016).

3.7.6. In-Vitro release studies

The release studies were performed for GRI loaded NS (F1) as well as for plain drug using USP dissolution tester apparatus II (Paddle method) (Hanson Research, Chatsworth, California, USA). The paddles rotated at 50 rpm and the temperature was kept at 37 °C ± 0.5 °C. Amounts of GRI loaded NS (F1) equivalent to 10 mg of drug as well as 10 mg pure drug were weighed and filled in dialysis bags. The dialysis bags (Molecular weight cut off 12,000–14,000 Da, Spectra/Pro, Spectrum Laboratories, Inc., USA) were tied with paddle and immersed in release medium. Initial release studies were conducted in 900 ml of 0.1 N HCl (pH = 1.2) for period of two hours, then the dialysis bags were transferred to 900 ml phosphate buffer pH 7.4 for the following five hours. Three ml samples were withdrawn after 0.25, 0.5, 0.75, 1, 2, 3, 4, 5, 6 and 7 hrs time intervals and replaced with an equal volume of fresh media. The samples were filtered and analyzed spectrophotometrically for GRI content at λ_{291nm}. The release studies were carried out in triplicate and then mean values were plotted as cumulative percent drug released against time.

Additionally, release profiles of GRI loaded NS (F1) and plain GRI were compared using difference factor (f_1) and similarity factor (f_2) and dissolution efficiency (DE).

Difference factor (f_1) and similarity factor (f_2) were calculated to compare between the release profiles using the following equations (FDA, 1997):

$$f_1 = \left[\frac{\left[\sum_{t=1}^{n}|R_t - T_t|\right]}{\sum_{t=1}^{n} R_t}\right] \times 100 \quad (4)$$

$$f_2 = 50.log\left\{\left[1 + \frac{1}{n}\sum_{t=1}^{n}(R_t - T_t)^2\right]^{-0.5}.100\right\} \quad (5)$$

where the f_1 calculates the percent difference between the two curves at each time point and is a measurement of the relative error between the two curves, n is the number of time points, $R_t$is the dissolution value of the reference (pure drug) at time t, and $T_t$is the dissolution value of the test at time t. The f_1 value of more than 15.0 and $f_2$value of less than 50 shows that the two profiles are dissimilar.

The dissolution efficiency (%DE) of a pharmaceutical dosage form is defined as the area under the dissolution curve up to a certain time, t, expressed as a percentage of the area of the rectangle described by 100% dissolution in the same time. It is calculated according to the following equation (Khan, 1975).

$$D.E. = \frac{\int_0^t y \times dt}{y_{100} \times t} \times 100\% \quad (6)$$

where y is the drug percent dissolved at time t. Dissolution efficiency (DE) % after 7 hrs was calculated for the formulae. Areas under the curves were calculated using the trapezoidal method.

3.7.7. Release kinetics and mechanisms

The *in-vitro* release data obtained were subjected to analysis for fitting to various kinetics models (zero order, first order, and Higuchi) as follows (Sharma et al., 2011):

$$\text{Zero order rate equation}: .Q_t = Q_0 + k_0 \quad (7)$$

where Q_t is the amount of drug released at time t, Q_0 is initial amount of drug, and K_0 is zero order release rate constant.

$$\text{First order rate equation}: \log Q = logQ_0 - \frac{k_1 t}{2.303} \quad (8)$$

where Q is the remaining amount of drug at time t, Q_0 is the initial amount of drug, K_1 is first order release rate constant, and t is time.

$$\text{Higuchi's model}: Q = K_H t^{1/2} \quad (9)$$

where Q is the amount of drug released in time t per unit area at time t, K_H is Higuchi diffusion rate constant.

The best-fitted model was selected based on the correlation coefficient (R^2) value.

To find out the mechanism of drug release from nanosponges, the in vitro release data of (F1) were fitted to Korsmeyer and Peppas equation (Korsmeyer et al., 1983):

$$\frac{M_t}{M_\infty} = kt^n \quad (10)$$

where, M_t/M_∞ is a fraction of drug release at time t, K is the release rate constant and n is the release exponent. The value of exponent (n) indicates the mechanism of drug release. The n value used for elucidation of drug release mechanism from GRI loaded nanosponges (F1) was determined from log cumulative percentage of drug release versus log time plots. Values of $n \leq 0.45$ indicate that drug release followed predominantly diffusion control mechanism (Fickian process) and drug diffusion through the NS is much faster than polymer chain relaxation. However, if $n \geq 0.89$, release follows non-Fickian or case II transport type mechanism. When, $0.45 < n < 0.89$, diffusion and release of drug occur in anomalous manner i.e. release is controlled by a combination of diffusion and polymer relaxation (Ritger and Peppas, 1987).

3.7.8. Evaluation of taste masking potential of GRI loaded nanosponges (F1)

Human panel gustatory response palatability studies were performed in healthy human volunteers (Juluri et al., 2016). The study proposal was approved by the Ethics Committee of Faculty of Pharmacy, Helwan University, No. 04H2019. The selection criteria being healthy human subjects with age range between 25 and 37 years old, whereas the exclusion criteria being subjects suffering from fever, cold, smokers, mouth sores, and wounds. For this purpose 6 human volunteers were selected. A sample of F1 equivalent to 150 mg was dispersed in 2 ml water to be held on the tounge/buccal cavity of each volunteer for 60 s and then volunteers were asked to evaluate F1 for taste bitterness. The bitterness level was recorded using a numerical scale (0–4) where 4 = very strong, 3 = strong, 2 = moderate, 1 = slight and 0 indicates no bitterness, respectively. The pure drug suspension (150 mg/2ml) was used as a standard control. Each of the volunteers was given the control, i.e., the pure drug suspension. They were asked to compare the bitterness of F1 with that of the control, indicating the level of bitterness perceived by them. The volunteers were instructed not to swallow the dose, which were placed on the tongue. As well as they were instructed to thoroughly gargle their mouth with distilled water after the completion of test. The scores given by all individuals were averaged and expressed as mean (±SD). The mean scores of pure drug suspension and the formula F1 were compared using *t*-test at 95% confidence level. $P < 0.05$ was considered statistically significant.

3.8. In-Vivo bioavailability study

The *in-vivo* bioavailability study was carried out to evaluate absorption of GRI loaded nanosponges (F1) formulation compared to oral GRI aqueous suspension.

3.8.1. Study design

An in vivo pharmacokinetic bioequivalence study was carried out to compare the rate and extent of absorption of GRI from GRI loaded nanosponge (F1) with GRI aqueous suspension. The study was a randomized, under fasting conditions. Fourteen healthy male albino rats with average body weight of 300±25 g were enrolled in the study. Rats were divided into 2 groups of 7 rats each. Rats of group (I) received single oral dose of the prepared GRI loaded nanosponge (F1) equivalent to 15 mg GRI /kg body weight (in form of 1 ml aqueous suspension). Rats of group (II) received single oral dose of pure drug suspension (1 ml) equivalent to 15 mg GRI /kg body weight (Dhanaraju et al., 1998). The preparations were administered orally to the rats along with 10 ml of water by using feeding tube. The protocol of the study was authorized by the Animal Ethics Committee of Faculty of Pharmacy, Helwan University, No. 24A2018 (Helwan, Egypt). Factors such as fluid intake, diet, posture, and physical activity were standardized as much as possible to limit their effects on gastrointestinal blood flow and motility (Torne et al., 2013). Water was allowed ad libitum except for 1 h before and after the dose administration. No food was allowed for 4 h after dosing; after which, the subjects were offered a standardized low-fat breakfast, and at 8 hrs post-dose, a standardized low-fat lunch was offered.

3.8.1.1. Blood sampling. Using the method adopted previously (Parasuraman et al., 2010); one ml orbital sinus blood samples were collected directly from each rat into heparinized tubes at zero (pre-dose), 1, 2, 3, 4, 8, 12, 24, 30, 36, 42 and 48 hrs post dose.

Plasma was immediately separated from the blood cells by centrifugation at 3000 rpm for 10 min and stored frozen at-80oC until required for analysis.

3.8.1.2. Analysis of plasma levels for Griseofulvin. Griseofulvin plasma levels were quantified using liquid chromatography – tandem mass spectrometry (LC-MS/MS) adapted from a reported method for GRI in plasma (Mistri et al., 2007). Internal standard [50 μl propranol hydrochloride (5 μg/ml)] was mixed with 200 μl plasma samples. Then the volume completed to 1 ml with acetonitrile. Samples were vortexed for 30 s then centrifuged at 3000 r.p.m. for 10 min. The upper layer was transferred to another tube, filtered through a 0.2 μm Millipore filter. Then 5 μl samples were injected onto the LC-MS/MS system. Calibration curves, ranging from 10 to 6000 ng/mL, were constructed by spiking blank plasma samples with serial dilutions of stock solutions of GRI for the quantitation of GRI in plasma samples.

3.8.1.3. LC-MS/MS system. LC-MS/MS system consisted of Agilent 6420 Triple Qua-druple with G1311A quaternary pump, G1329A auto-sampler, and G1322A vacuum degasser (Agilent Technologies Deutschland GmbH, Waldbron, Germany). The analytical column was intersil ODS-3 (50 mm × 4.6 mm, *dp* 5 μm, Sigma–Aldrich). The mobile phase consisted of acetonitrile: 0.05% formic acid in water (70:30, %v/v) for isocratic elution. The flow rate was adjusted at 0.3 ml/min under ambient temperature. The injection volume was 5 μl. The operation mode was electro-spray positive mode. Gas temperature was 350 °C and nitrogen gas flow rate was 10 L/min. Nebulisation pressure was 40psi and capillary voltage was 4000v. Quantitation of the transitions from *m/z* 353 to 165 for (GRI) and from *m/z* 260.1 to 116.2 for the internal standard (propranolol hydrochloride), respectively was conducted with a scan time of 1.1 min. Data acquisition was performed using 6400 Series Triple Quadrupole B.07.00 (version B7022.0) software.

3.8.2. Assay validation

3.8.2.1. Preparation of GRI calibation curve in rat plasma. Drug – free rat plasma samples of 200 μl volume were spiked with different aliquots of GRI methanolic stock solution (200,000 ng/mL). Then 50 μl propranolol hydrochloride solution (5 μg /ml) was added as internal standard. Then the volume was completed to 1 ml with acetonitrile to precipitate plasma protein producing concentrations of 10, 20, 50, 100, 250, 500, 1500, 4000, 6000 ng/mL. All samples were vortexed for 30 s and centrifuged at 3000 rpm for 10 min. The upper layer was transferred to another tube, filtered through a 0.2 μm millipore filter. Then 5 μl samples were injected onto the liquid chromatography. Peak area ratios of GRI / propranolol hydrochloride (internal standard) were utilized for the construction of calibration curve; using weighted ($1/x^2$) linear least squares regression of the plasma concentrations and the measured peak area ratios.

3.8.2.2. Accuracy and precision. The accuracy (% recovery) of the assay was assessed by comparing the peak area ratios (GRI/propranlol hydrochloride) of quality control (QC) samples (spiked plasma before protein precipitation) of three drug concentrations; 30 ng/ml (low quality control, LQC); 2500 ng/ml (medium quality control, MQC) and 5000 ng/ml (high quality control, HQC) to the peak area ratios for drug free plasma samples (spiked after protein precipitation) at each QC level. The precision of the assay was measured as the relative standard deviation% (RSD %) for the recovered concentrations. For determining the intra-day accuracy and precision, replicate analysis of plasma samples of GRI was performed on the same day. The run consisted of a calibration curve and three replicates of LQC, MQC and HQC samples. The inter-day accuracy and precision were assessed by analysis of three precision and accuracy batches on three consecutive validation days.

3.8.2.3. Pharmacokinetic analysis. The pharmacokinetic parameters (PKPs) following oral administration of the treatments were estimated for each rat in each group. The values of the maximum griseofulvin plasma concentration (C_{max}, ng/ml), the time to reach C_{max} (T_{max}, hr), the area under the plasma-concentration time curve from time zero to 48 hr (AUC $_{0\text{-}48}$, ng.hr/ml), elimination rate constant ($K_{el,}$ hr^{-1}) and elimination half–life ($t_{1/2}$, hr) were calculated from plasma concentrations of GRI vs. time using the non-compartmental method.

The values of the C_{max} and T_{max} were obtained directly from plasma data while the area under the plasma-concentration time curve ($AUC_{0\text{-}48}$, ng.hr/ml) was calculated using the log-linear trapezoidal rule method. Elimination rate constant (k_{el}) was calculated from the slope of the terminal part of the concentration- time curve where the slope = $-k_{el}$ /2.303 then half-life ($t_{1/2}$) was calculated as 0.693/ k_{el}. All PKPs were calculated using the Thermo Scientific™ Kinetica software version 5.1 (ThermoFisher Scientific, Waltham, MA, USA).

3.9. Statistical analysis

Descriptive statistics for the pharmacokinetic parameters were reported. The obtained pharmacokinetic parameters (C_{max}, AUC $_{0\text{-}48}$, K_{el} and $t_{1/2}$) were analyzed by student unpaired *t*-test using Microsoft office 2007, Excel package. A statistically significant difference was considered at $P < 0.05$. On the other hand, T_{max} values were analyzed using the non-parametric Mann-Whitney test using GraphPad Instat® (version 3.05). A statistically significant difference was considered at $P < 0.05$.

3.9.1. Establishment of in-vitro/in-vivo correlation (IVIVC)

For drugs of BCS Class II as GRI, *in-vivo* dissolution is the rate-limiting step of *in-vivo* absorption and bioavailability. Therefore, bio-reflective *in-vitro* dissolution methodologies are encouraged in order to assure the bioequivalence standards (Tsume et al., 2014). Level A of IVIVC has been selected to represent point to point correlation between the in-vitro fraction dissolved of GRI from F1 and the in-vivo response as fraction of GRI absorbed from F1 using Wagner-Nelson method (Sankalia et al., 2008; Shah et al., 2009). The fractions of GRI absorbed from F1 obtained were plotted against the fraction of GRI dissolved from F1 at the same time and the correlation coefficient (r^2) was determined.

4. Results and discussion

4.1. Percent yield of plain β-CD NS

The percent yield of different nanosponges (NS1, NS2 and NS3) was shown in Table 2. The percent yield of nanosponges was found to be lowest for the molar concentration (1:2). This might be due to low concentration of the cross linker (diphenylcarbonate) which prevent the formation of completed network of nanosponge (Rao et al., 2013). Higher percent yield was provided at higher molar ratios (1:4 and 1:6). However, the yield was found to be almost

Table 2
Percent yield of different types of NS.

Percent Yield (%) ± SD, n = 3	(β-CD:DPC) Molar ratio	Type of NS
21.30 ± 0.021	1:2	NS1
32.79 ± 0.091	1:4	NS2
32.90 ± 0.11	1:6	NS3

same at both concentrations. This might be due to saturation of the reactive functional groups at higher concentration. That primary hydroxy groups are mainly involved in the formation of nanosponges (Castiglione et al., 2013). Based on these results, NS1 excluded from further assessment in this study.

4.2. Construction of the GRI - β cyclodextrin as well as GRI-NS (NS2 and NS3) phase solubility diagrams

Fig. 1 represents the phase solubility diagram of GRI in solutions of different concentrations of β-CD in distilled water. According to Higuchi and Connors (Higuchi and Connors, 1965), the phase solubility profile of GRI with β-CD was classified as Higuchi's B_s-type since the initial rising portion was followed by plateau. This indicated the limited solubility of the GRI -β-CD complex. This might be due to the limited solubility of β-CD in aqueous media. The stoichiometric ratio of GRI with β-CD was 1:1 as the slope of curves were less than unity (0.033) (Higuchi and Connors, 1965).

Estimation of the apparent stability constant (K_C) of GRI-β-CD complex is important since it is an index of changes of physicochemical properties of a compound upon complexation. The stability constant (K1:1) of the complexes is indicative of the strength of interaction between the host and guest. In supramolecular interactions, the Kc in the range of 200–5000 M^{-1} signifies strong interactions between the host and guest (Del Valle, 2004). The stability constant (Kc) for GRI-β-CD was estimated by the following equation (Higuchi and Connors, 1965).

$$k1:1 = \frac{slope}{S_0(1 - slope)} \quad (11)$$

The calculated Kc for GRI-β-CD was 975.03 M^{-1}. Thus, indicating a reasonably strong interaction between the host (β-CD) and guest (GRI).

Fig. 2 represents the phase solubility diagram of GRI in the distilled water solutions of different concentrations of NS2 and NS3. The solubility phase diagram of NS2 showed increase in GRI aqueous solubility as a function of the concentration of NS2 (up to 2%w/v). Also, the solubility phase diagram of NS3 showed an initial increase in GRI aqueous solubility as a function of the concentration of NS3 (up to 1.4 %w/v) followed by slight increase in solubility with increase in NS3 concentration up to 2%w/v (plateau). Moreover, it was found that the maximum achieved values for GRI solubility in this study were 0.4792 ± 0.128, 0.840 ± 0.090 and 0.592 ± 0.087 mM for β-CD, NS2 and NS3 respectively, while, the inherent solubility of GRI was nearly 0.035 ± 0.003 mM. The solubility enhancement factors were calculated and it was found that GRI solubility was enhanced 13.69, 24 and 16.91 folds in case of β-CD, NS2 and NS3, respectively. Thus, solubility studies showed that solubility of GRI was more enhanced with the presence of both NS2 and NS3 compared to native β-CD. However, the extent of

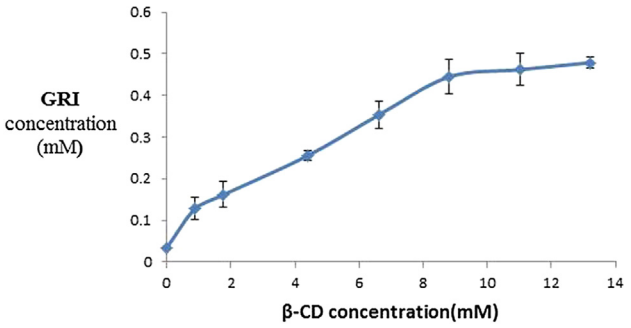

Fig. 1. Phase solubility diagram for GRI/β-CD (37° ± 0.5 °C).

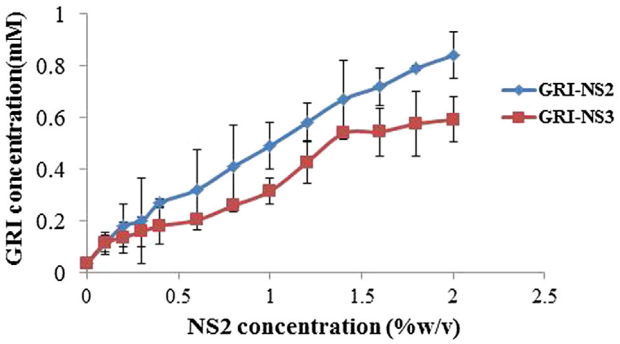

Fig. 2. Phase solubility diagram for GRI-NS2 and GRI-NS2 (37° ± 0.5 °C).

increase in solubility was more remarkable for NS2 (β-CD: DCP = 1:4). Increasing concentration of cross linker in NS3 (β-CD: DCP = 1:6) might lower the affinity of nanosponge to interact with the drug. This result was in agreement with previously reported results (Rao et al., 2013). The authors found that dissolution of telmisartan from nanosponges synthesized using 1:6 β-CD: crosslinker ratio was lower than from nanosponges synthesized using 1:4 β –CD: crosslinker. This might be due to the too high increase in degree of cross-linking and creation of more complex and tortuous nanochannels at 1:6 ratios which prevent the entrapment of the drug into the nanosponge structure (Rao et al., 2013). Hence, the NS2 synthesized using 1:4 β –CD: crosslinker ratio was found to have a desirable impact on the solubility profile. Hence further studies were conducted using NS2.

4.3. Molecular modeling studies for prediction of the best binding mode of griseofulvin by docking study

According to the docking results, griseofulvin showed many hydrogen bonds that fixed its fitting and confirmed its high affinity as shown in Fig. 3. The free energy of binding of griseofulvin was −21.35 kcal/mol that was much better than the reported resveratrol −18.11 kcal/mol.

4.4. Determination of percentage of drug loading in the prepared NS

The percentage drug loading was determined for all nanosponges formulae (F1-F8) as listed in Table 3. The drug content

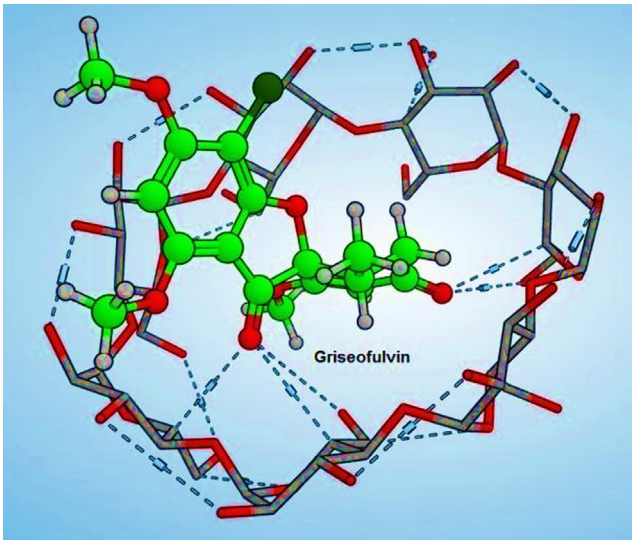

Fig. 3. 3D image showing possible mode of entrapment of GRI in NS structure.

Table 3
Percentage of drug loading of GRI-NS formulae.

Formula No	Percentage drug loading (%) ± SD, n = 3
F1	47.20 ± 0.38
F2	36.83 ± 0.7
F3	30.34 ± 0.43
F4	20.20 ± 0.82
F5	33.90 ± 0.41
F6	21.00 ± 0.52
F7	27.60 ± 0.80
F8	22.90 ± 0.28

was observed to be higher for the formulae contained 0.25%w/w PVP K30 compared to their counterparts lacking PVP K30. It was reported that the encapsulating properties of CDs can be improved by forming ternary complexes. The ternary complexes are supramolecular systems composed of three distinct molecular entities. From this point of view, this ternary system would be represented by an auxiliary substance which, in conjunction with CD, can improve the physicochemical, chemical and bioavailability properties of a guest molecule. Depending on the case, the use of a third component improves encapsulation or release and reduces the amount of CD needed to obtain the benefits mentioned above. In this way can optimize the cost, toxicity, and bulk formulation of the desired product (Folch-Cano et al., 2014). Hydrophilic polymers have been used in the recent past for enhancing the complexation efficiency of β- CDs (Loftsson and Brewster, 1996; Loftsson et al., 2005; Patel and Vavia, 2006; Sami et al., 2010). This might be attributed to the establishment of different interactions with CDs and drug molecules such as hydrophobic bonds, Van der Waals forces, or hydrogen bonds. Polymers are known to interact with the outer surface of CDs and with drug-CD complexes, forming aggregates or co-complexes i.e., a complex between several drug–CD molecules and a polymer chain [(drug–CD)n–polymer] that increase the complexation efficiency (Challa et al., 2005; Ribeiro et al., 2003). With the same rational hydrophilic polymer copolyvidonum (copolyvinylpyrrolidone) was used with β-CD nanosponges as an auxiliary component to enhance the complexation efficiency and inclusion of itraconazole in β-CD nanosponges (Swaminathan et al., 2007). Moreover, efavirenz, a non-nucleoside reverse transcriptase inhibitor with a low aqueous solubility, was loaded in βCD-NS to improve its solubility. For this purpose, a ternary system, comprising drug-loaded βCD-NS and polyvinylpyrrolidone 30 K was prepared. This ternary system produced a two fold increase in the bioavailability of efavirenz in comparison to the free drug after oral administration to rats (Rao and Shirsath, 2017)**.** In this study, among the prepared fourteen GRI loaded nanosponges (F1-F8), the formula F1 achieved the highest percentage drug loading 47.2 **±** 0.38%. Thus, this formula was selected for further assessment studies.

4.5. Characterization of the selected GRI loaded NS formula (F1)

4.5.1. Scanning electron microscopy examination (SEM)

The SEM image in Fig. 4 revealed the highly porous structure of GRI loaded NS formula (F1) indicating sponge - like shape. The porous texture of the nanosponge facilitates the infiltration of the drug into the interpenetrating network of the nanosponge.

4.5.1.1. Determination of particle size, polydispersity index (PDI) and zeta potential. Particle size and surface charge are amongst the key criteria governing the biological behavior of oral nano-platforms; having a great impact on stability, in vivo distribution, bioavailability, metabolism, elimination, and toxicity (Alexis et al., 2008).

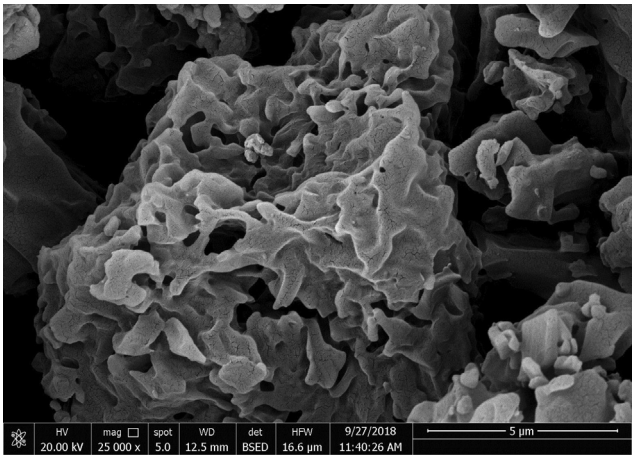

Fig. 4. Scanning electron microscopy (SEM) image of GRI loaded NS formula (F1).

The average particle sizes of the formulae (F1) were found to be 665.9 ± 13.8 nm. The polydispersity index was 0.367 ± 0.002. The zeta potential of (F1) was found to be (-21.50 ± 0.7 mV) which was considered to be quite sufficient for keeping individual particles well–separated from each other as a result of electric repulsion. The negative charge was attributed to carbonyl groups and the free hydroxyl groups of β–CD (Zidan et al., 2018).

4.5.1.2. Differential Scanning Calorimetry (DSC). The DSC spectra of GRI showed a sharp melting endothermic peak at 219.6 °C. The DSC thermograms of F1 did not show the melting peak corresponding to drug fusion, Fig. 5. This indicated that the drug was no longer crystalline and could be molecularly dispersed in nanosponge. Also, this could confirm encapsulation and interaction of GRI with the NS2 structure by inclusion as well as non-inclusion phenomenon (Ansari et al., 2011). Moreover, F1 shows the melting peak corresponding to PVP fusion, Fig. 5.

4.5.1.3. Fourier Transform Infrared (FT-IR) spectroscopy. Fig. 6 shows the FT-IR spectra for GRI, β-CD, PVP, plain NS2 and F1. The FT-IR spectra of plain NS2 exhibited a prominent peak at 1774.5 cm^{-1}, which is an indicative of carbonyl bond between β-CD units (Rao and Bhingole, 2015). It was evident from the reported spectra that this peak was absent in the FTIR spectrum of β–CD. The spectrum

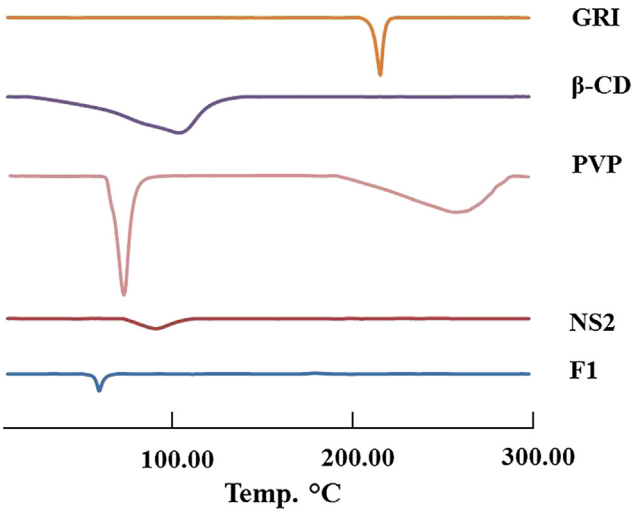

Fig. 5. DSC Thermograme of GRI, β-CD, PVP, plain NS2 and F1.

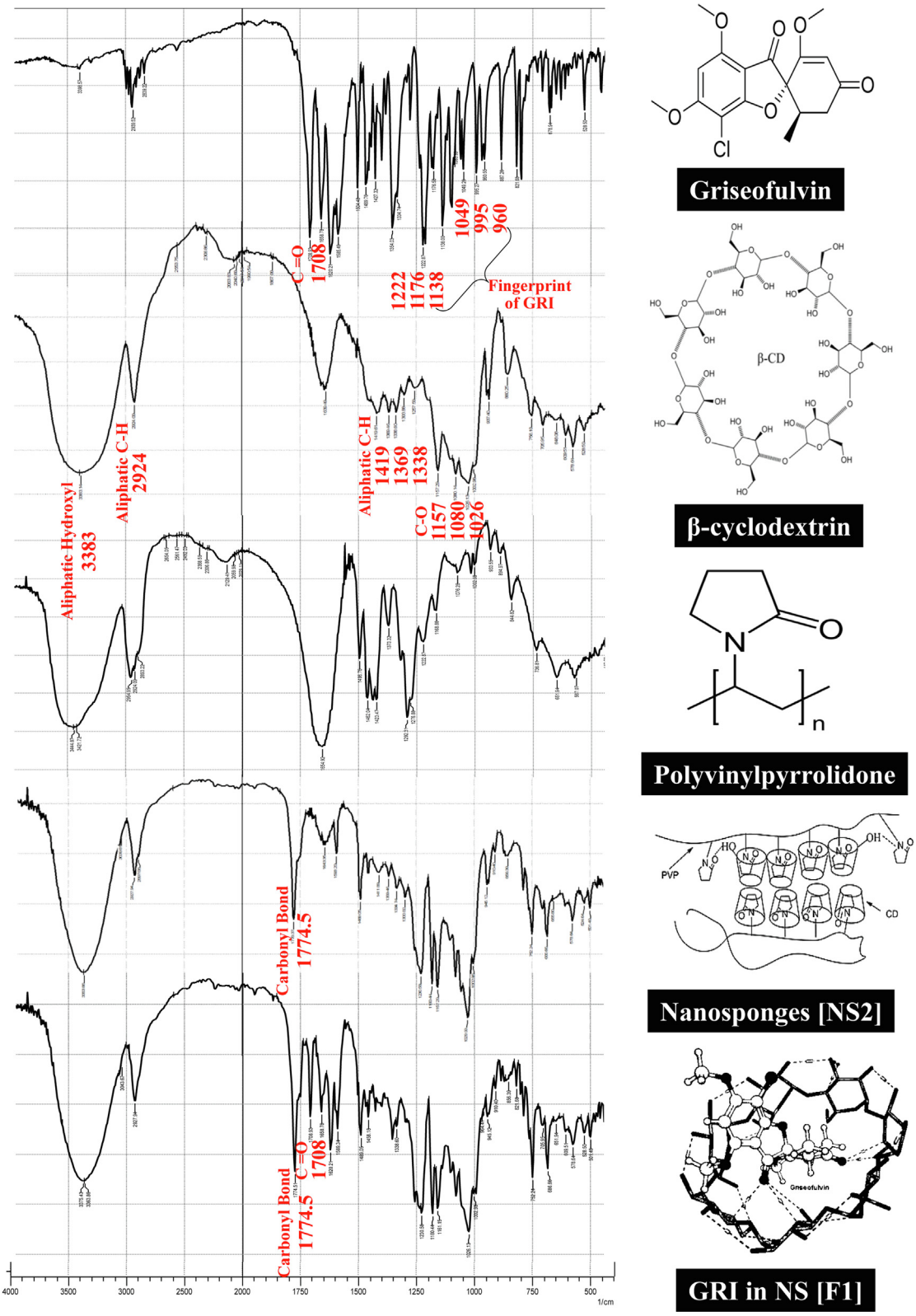

Fig. 6. FT-IR spectra of GRI, β-CD, PVP, plain NS2 and F1.

of β-CD was characterized by a peak at 3383 cm^{-1} which represents the aliphatic hydroxyl group. Strong peaks at 2924, 1419, 1369 and 1338 cm^{-1} were observed due to aliphatic C—H. Peaks were found at 1157, 1080 and 1026 cm^{-1} due to C—O group. The region from 1000 till 405 cm^{-1} represented a characteristic finger print for the compound. The spectrum of F1 showed that all characteristic peaks of griseofulvin were still present even after its complexation such as: C=O at 1708 cm^{-1} (wave number is decreased due to its conjugation with C=C). In addition, C=C bending at 1466 and 1660 cm^{-1} of benzene ring, C—O bending at

1223 cm^{-1} as well as C—Cl bending at 822 cm^{-1}. The suggested cause for the apparent change in fingerprint region(disappearance peaks of GRI at 1222 cm^{-1}, 1176 cm^{-1}, 1138 cm^{-1}, 1049 cm^{-1}, 995 cm^{-1} and 960 cm^{-1}) and the apparent change in peak intensity was the complexation of the drug to complexing agent by hydrogen bond (broadening of peaks) between carbonyl oxygen of the drug and polar hydrogens of the complexing agent. In addition to Wander-Waal's interaction between OCH_3 group of the drug and

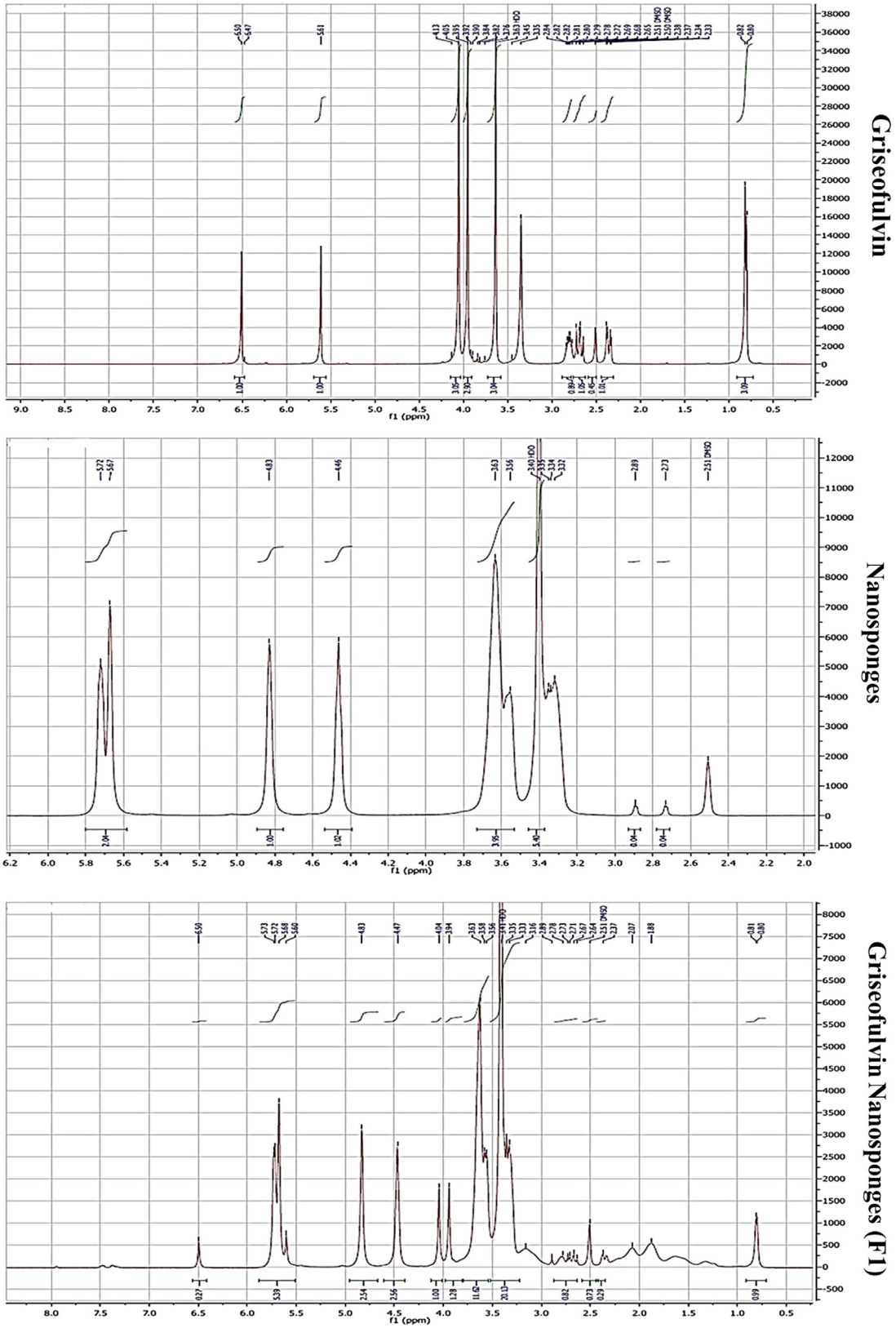

Fig. 7. NMR spectra of GRI, plain NS2 and F1.

complexing agent and Dipole-Dipole interaction, a comparison of FTIR spectra of resveratrol and reversatrol- NS complex was carried out and showed that there were major changes in the fingerprint region, (i.e., 900 to 1400 cm^{-1}) indicating drug loading in nanosponges (Ansari et al., 2011).

4.5.1.4. Nuclear Magnetic Resonance (NMR) spectroscopy. Fig. 7 shows the H1-NMR spectrum of the characteristic peaks of Griseofulvin (a), Nanosponge (b) and the formula F1(c). The intensity of peak of aromatic protons at 6.5 ppm of Griseofulvin (a) was reduced in F1(c) (Salazar et al., 2018), also it was noticeable the shift of olefinic protons peak of Griseofulvin at 5.6 ppm to 5.5 ppm in F1(c) which appeared with that of Nanosponges at 5.5 as splitting peaks. Also shift was occurred at peaks appeared from 3.2 to 3.8 ppm for Griseofulvin to 3.3 to 4.1 ppm in F1

Proton signals from the guest molecules showed high-field chemical shifts in F1, possibly due to screening effects caused by the spatial restriction of the Griseofulvin included inside the cavities of the NS, these chemical shifts, confirming the complexation (Mele et al., 2011; Olteanu et al., 2015; Salazar et al., 2018).

4.6. In-Vitro release studies

As illustrated in Fig. 8, the *in-vitro* release profile of GRI from formulation F1 was evaluated in comparison to the plain GRI. The *in vitro* release GRI from F1 as well as plain GRI was carried out in 0.1 N HCl for the first two hrs followed by phosphate buffer pH 7.4 for the following five hrs.

In 0.1 N HCl, the GRI cumulative percent released from F1 after 2 hrs was 72.3 ± 0.24% while the percentage of cumulative dissolution of the plain GRI was 21.81 ± 0.07%. After 5 hrs in pH 7.4 (7 h from the start of the expermint), GRI was released completely from F1 while the percentage of cumulative dissolution of the plain GRI was only 27.43 ± 0.32%. The comparison between dissolution profiles of plain GRI and F1 based on calculating both difference factor (f_1) and similarity factor (f_2). The calculated difference factor (f_1) was 187.12 (more than 15) and similarity factor (f_2) was 15.33 (less than 50) indicated that the two profiles are dissimilar and the encapsulation of GRI in NS resulted in a remarked increase in its extent of drug release. Moreover, it was clear that F1 exhibited higher release characteristics than plain GRI through calculating the dissolution efficiency (%D.E.). The %D.E. were 23.87% and 76.18% for plain drug and F1 formula, respectively. Thus, the formulation of the drug as nanosponges resulted in 3.19 folds enhancement in dissolution efficiency (% D.E.). This could be due to the potential of nanosponges to enhance the dissolution of poorly soluble drugs by entrapping them within their nanochannels and cavities, and thus masking their hydrophobic moieties and increasing their apparent solubility (Ansari et al., 2011; Mognetti et al., 2012; Swaminathan et al., 2007). Inaddition, encapsulation of hydrophobic drugs into NS causes a reduction of crystallinity and enhanced wettability which helps solubilizing drugs and maintaining a higher fraction in a molecularly dispersed state. Therefore, the *in vitro* release results of GRI-loaded NS (F1) suggested a promising efficacy on improving GRI bioavailability by enhancing its poor dissolution after administration. Moreover, the enhanced dissolution property of nanosponges can be described by Noyes-Whitney equation.

$$\frac{D_C}{d_t} = D.A/h(cs - cx) \tag{12}$$

where, D is the diffusion coefficient, A the surface area, cs is the saturation solubility, cx the bulk concentration, and h is the so-called "diffusional distance" over which the concentration gradient occurs. It is obvious that an increase in the surface area consequently increases the dissolution velocity. In addition, drug nanoparticles are characterized by an increase in saturation solubility cs. According to Noyes–Whitney, the increase in cs—in addition to the enlarged surface area—further increases the dissolution velocity. The simultaneous increase in saturation solubility cs leads to an increased concentration gradient (cs − cx), thus enhancing the dissolution velocity in addition to the surface effect. The dissolution velocity is reversely proportional to the diffusional distance h, which means that reducing h leads to a further increase in dissolution velocity. According to the Prandtl equation (Muller and Keck, 2004). The diffusional distance h decreases for very small particles. Additionally, the inclusion of a third component (PVP) in F1 could exert synergistic effect on drug solubility and release from nanosponges. Swaminathan *et al.* have studied nanosponges with itraconazole, a drug with aqueous solubility of about 1 ng mL^{-1} at physiological pH. Incorporation of the drug in nanosponges improved the drug's solubility by 27 times and on adding PVP as an auxiliary component in the nanosponge formulation, the solubility was enhanced to 55-folds (Swaminathan et al., 2007).

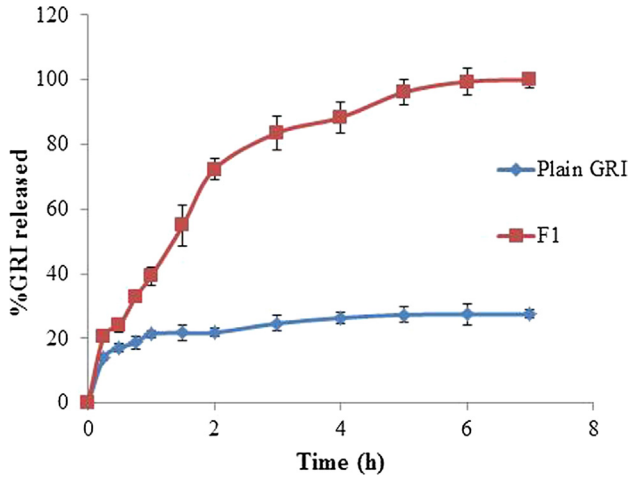

Fig. 8. *In-vitro* release profiles of GRI from plain GRI and the selected GRI loaded nanosponges (F1).

4.6.1. Release kinetics and mechanisms

The *in vitro* release data for both plain GRI and F1 fitted best to Higuchi release kinetics model based on the highest correlation coefficient (R^2) value. The mechanism of GRI *in vitro* release from the prepared formula F1 were studied by applying the Korsmeyer –Peppas model to the release data up to 60%. The GRI loaded nanosponges (F1) had (n) value of 0.546 indicating a non-fickian model (anomalous transport) where release is controlled by a combination of diffusion and polymer chain relaxation.

4.7. Evaluation of taste masking potential of GRI loaded nanosponges (F1)

The results from the human panel gustatory response palatability studies demonstrated a significant difference ($P < 0.05$) in the bitterness score between the GRI nanosponges formula (F1) and the plain GRI suspension. That, the plain GRI suspension revealed strong bitter taste with average score of 3.83 ± 0.41. While, the GRI nanosponges (F1) showed a mean bitterness score 0.00 ± 0.00. Thus, the results of the human panel studies confirmed the potential of GRI nanosponges (F1) in masking the bitter taste of griseofulvin completely.

4.8. In-Vivo bioavailability study

The described LC-MS/MS assay was proved to be sensitive, accurate and reproducible with lower limit of quantification of 10 ng/mL for Griseafulvin. The assay showed good linearity in the range of concentration (10–6000 ng/mL) with regression coefficient 0.999. The mean % recovery for intra and inter quality control samples ranged from 94.93 −104.20% and 93.90–99.90%, respectively indicating high accuracy of the assay. Also, RSD% of all intra and inter quality control samples were less than 15% reflecting a high degree of intra and inter day precision of the assay.

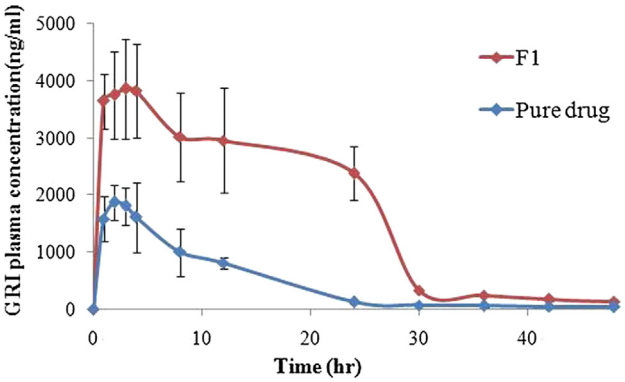

Fig. 9. Mean plasma concentration–time curves of griseofulvin in rats after single oral administration of (15 mg/kg GRI) of the prepared GRI loaded nanosponge (F1) and pure drug.

Fig. 9 illustrates the mean GRI plasma concentration–time curves after oral administration of single dose (15 mg GRI /kg) of the prepared GRI loaded nanosponge (F1) and pure drug suspension to rats. Table 4 shows pharmacokinetic parameters (mean values of C_{max}, T_{max}, AUC $_{0\text{-}48}$, k_{el} and $t_{1/2}$) for the prepared GRI loaded nanosponge (F1) and pure drug suspension, respectively,

Statistical analysis of the pharmacokinetic parameters revealed that the difference between the k_{el} and $t_{1/2}$ values of both F1 formulation and pure drug was statistically insignificant (P>0.05). However, there was a significant difference ($P < 0.05$) between values of C_{max}, T_{max} and AUC $_{0\text{-}48}$. The mean C_{max} and AUC $_{0\text{-}48}$ in the group administered F1 was 2.13 and 3.78 folds higher than the group administered the pure drug, respectively. The statistically significant ($P < 0.05$) higher C_{max} and $AUC_{0\text{-}48}$ that produced by the prepared GRI loaded nanosponges (F1) ensured that the oral bioavailability of GRI was improved by complexation of GRI with

Table 4
Pharmacokinetic parameters following single oral dose administration of the prepared GRI loaded nanosponge (F1) and pure drug equivalent to 15 mg/kg GRI, to fourteen healthy male albino rats.

Parameter	GRI Loaded Nanosponge (F1)		Pure Drug	
	Mean	±SD	Mean	±SD
C_{max} (ng/mL)	3855.32	± 870.71	1809.11	± 328.25
T_{max} (h)*	3*	(1) **	2*	(0.5) **
$AUC_{0\text{-}48}$ (ng.h/mL)	84865.64	± 11394.16	22466.90	± 4649.40
k_{el} (h^{-1})	0.044	± 0.002	0.037	± 0.011
$t_{1/2}$ (h)	15.87	± 0.84	20.03	± 6.48
* Median & range				
**Interquartile range				
C_{max}	*= Maximum plasma concentration*			
T_{max}	*= Time to maximum plasma concentration*			
$AUC_{0\text{-}48}$	*= Area under the plasma concentration – time curve to last measurable concentration*			
k_{el}	*= Elimination rate constant*			
$t_{1/2}$	*= Elimination half-life*			

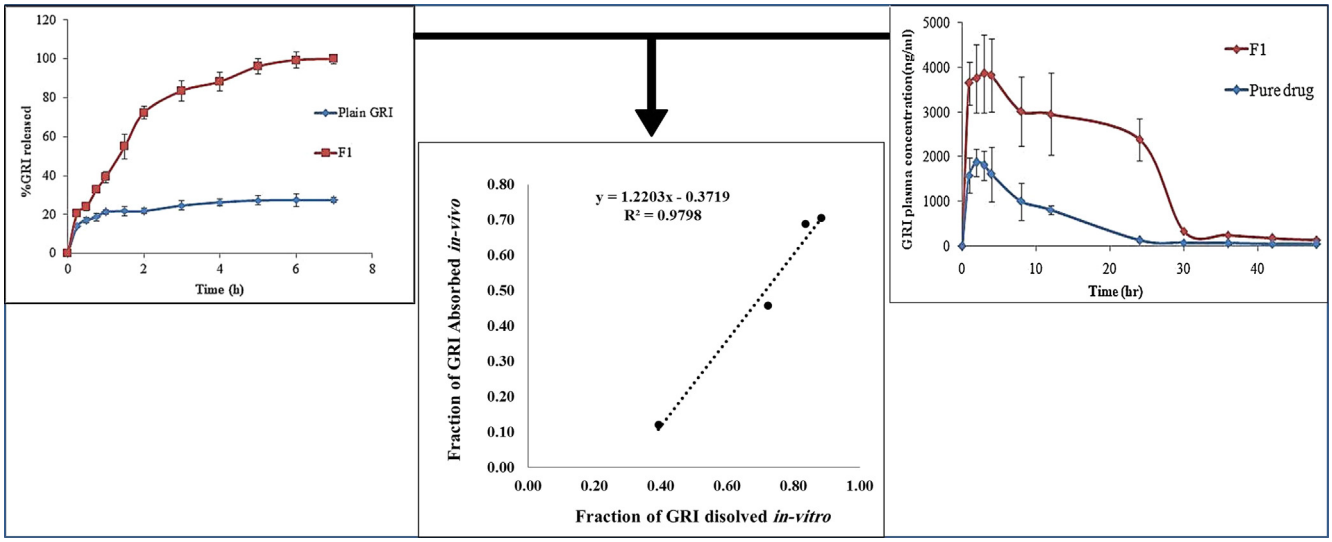

Fig. 10. *In Vitro*/*In-vivo* data correlation (IVIVC) of GRI from F1.

nanosponges. This could be attributed to the improved solubility and dissolution rate of F1 compared to the pure drug. It could be noticed from the results that the enhancement factor of AUC_{0-48} achieved by nanosponges (F1) was a reflection for the enhancement factor of dissolution efficiency%. As the Nanosponges (F1) provided 3.19 folds increase in dissolution efficiency%, an increase of 3.78 folds in AUC_{0-48} was achieved. The statistically significant ($P < 0.05$) prolongation in T_{max} of F1 might be due to the presence of the drug in the nanocavities of the nanosponges and the inclusion phenomenon of the cyclodextrin (Mady et al., 2018).

5. Establishment if in vitro/in vivo correlation (*IVIVC*)

The determination of *IVIVC* is essential to present the ability of in-vitro dissolution characteristics in predicting the in-vivo bioequivalence of a drug product (Sankalia et al., 2008). Fig. 10 illustrates the linear correlation plot of fraction of GRI absorbed vs. fraction of GRI dissolved of F1 formula. Talented point to point relationship was obtained with correlation coefficient of 0.9798 which designated a close correlation between GRI *in-vitro* dissolution rate and its *in-vivo* absorption.

6. Conclusion

The current study, successfully developed GRI loaded nanosponges to mask the bitter taste of GRI, improve dissolution rate and eventually enhance oral bioavailability. Solubility phase diagram aided in the selection of 1:4 (NS2) as the most appropriate ratio of β–CD to the crosslinker diphenyl carbonate that could be used for GRI loading. The formula (F1) composed of 1:1 w/w (NS2: GRI) along with 0.25%w/w PVP k30 provided highest drug loading capacity and showed promising *in-vitro* release with 3.19 folds increase in dissolution efficiency %. Human panel gustatory response palatability studies confirmed the potential of F1 for GRI bitter taste masking. Moreover, Improvement in bioavailability was observed in rats as there was 2.13 and 3.78 folds increase in C_{max} and AUC_{0-48}, respectively compared to plain GRI. Thus, the formula F1 could be used as a successful GRI dosage form for pediatrics in form of dry suspension for reconstitution. However, further *in-vivo* absorption studies in humans and clinical investigations in patients should be carried out to support the obtained results.

Acknowledgement

We express our gratitude to Associate Prof. Dr. Mohammed abdou khedr, associate professor of medicinal chemistry and drug design, Department of Pharmaceutical Chemistry, Faculty Of Pharmacy, Helwan University for his help in performing molecular docking study.

Declaration of Competing Interest

The authors report no conflicts of interest.

References

Ahuja, A., Baboota, S., Ali, J., Mustafa, G., 2011. Cyclodextrins as potential excipients in pharmaceutical formulations: solubilizing and stabilizing effects. Cyclodextrins Pharm. Cosmetics Biomed.: Curr. Fut. Industr. Appl., 19–43

Alexis, F., Pridgen, E., Molnar, L.K., Farokhzad, O.C., 2008. Factors affecting the clearance and biodistribution of polymeric nanoparticles. Mol. Pharm. 5 (4), 505–515.

Amidon, G.L., Lennernäs, H., Shah, V.P., Crison, J.R., 1995. A theoretical basis for a biopharmaceutic drug classification: the correlation of in vitro drug product dissolution and in vivo bioavailability. Pharm. Res. 12 (3), 413–420.

Ansari, K.A., Vavia, P.R., Trotta, F., Cavalli, R., 2011. Cyclodextrin-based nanosponges for delivery of resveratrol: in vitro characterisation, stability, cytotoxicity and permeation study. AAPS PharmSciTech 12 (1), 279–286.

Arida, A.I., Al-Tabakha, M.M., Hamoury, H.A.J., 2007. Improving the high variable bioavailability of griseofulvin by SEDDS. Chem. Pharm. Bull. 55 (12), 1713–1719.

Bennett, M.L., Fleischer Jr, A.B., Loveless, J.W., Feldman, S.R., 2000. Oral griseofulvin remains the treatment of choice for tinea capitis in children. Pediatr. Dermatol. 17 (4), 304–309.

Castiglione, F., Crupi, V., Majolino, D., Mele, A., Panzeri, W., Rossi, B., Trotta, F., Venuti, V., 2013. Vibrational dynamics and hydrogen bond properties of β-CD nanosponges: an FTIR-ATR, Raman and solid-state NMR spectroscopic study. J. Incl. Phenom. Macrocycl. Chem. 75 (3–4), 247–254.

Cavalli, R., Trotta, F., Tumiatti, W., 2006. Cyclodextrin-based nanosponges for drug delivery. J. Incl. Phenom. Macrocycl. Chem. 56 (1–2), 209–213.

Challa, R., Ahuja, A., Ali, J., Khar, R.K., 2005. Cyclodextrins in drug delivery: an updated review. AAPS PharmSciTech 6 (2), E329–E357. https://doi.org/10.1208/pt060243.

Chiang, P.-C., Cui, Y., Ran, Y., Lubach, J., Chou, K.-J., Bao, L., Jia, W., La, H., Hau, J., Sambrone, A., 2013. In vitro and in vivo evaluation of amorphous solid dispersions generated by different bench-scale processes, using griseofulvin as a model compound. AAPS J. 15 (2), 608–617.

Dandagi, P.M., Kaushik, S., Telsang, S., 2011. Enhancement of solubility and dissolution property of griseofulvin by nanocrystallization. Int J Drug Dev Res 3, 180–191.

Dash, A.K., Mishra, D., 2012. Method development, validation and stability study of griseofulvin in bulk and pharmaceutical dosage form by UV-spectrophotometric method. Asian J. Pharm. Res. 2 (1), 66–69.

Del Valle, E.M., 2004. Cyclodextrins and their uses: a review. Process Biochem. 39 (9), 1033–1046.

Dhanaraju, M., Kumaran, K.S., Baskaran, T., Moorthy, M.S.R., 1998. Enhancement of bioavailability of griseofulvin by its complexation with β-cyclodextrin. Drug Dev. Ind. Pharm. 24 (6), 583–587.

Dua, K., Pabreja, K., Ramana, M., Lather, V., 2011. Dissolution behavior of β-cyclodextrin molecular inclusion complexes of aceclofenac. J. Pharm. Bioallied Sci. 3 (3), 417–425.

FDA, 1997. Guidance for Industry: Dissolution Testing of Immediate Release Solid. Dosage Forms, Oral.

Folch-Cano, C., Yazdani-Pedram, M., Olea-Azar, C., 2014. Inclusion and functionalization of polymers with cyclodextrins: current applications and future prospects. Molecules 19 (9), 14066–14079.

Furniss, B.S., 1989. Vogel's textbook of practical organic chemistry. Pearson Education India.

Higuchi, T., Connors, K.A., 1965. Phase solubility techniques. Anal. Chem. Instr. 4, 117–212.

Juluri, A., Popescu, C., Zhou, L., Murthy, R.N., Gowda, V.K., Kumar, C., Pimparade, M. B., Repka, M.A., Murthy, S.N., 2016. Taste masking of griseofulvin and caffeine anhydrous using Kleptose Linecaps DE17 by hot melt extrusion. Aaps Pharmscitech 17 (1), 99–105.

Khan, K., 1975. The concept of dissolution efficiency. J. Pharm. Pharmacol. 27 (1), 48–49.

Korsmeyer, R.W., Gurny, R., Doelker, E., Buri, P., Peppas, N.A., 1983. Mechanisms of solute release from porous hydrophilic polymers. Int. J. Pharm. 15 (1), 25–35.

Loftsson, T., Brewster, M.E., 1996. Pharmaceutical applications of cyclodextrins. 1. Drug solubilization and stabilization. J. Pharm. Sci. 85 (10), 1017–1025. https://doi.org/10.1021/js950534b.

Loftsson, T., Össurardóttir, Í.B., Thorsteinsson, T., Duan, M., Másson, M., 2005. Cyclodextrin solubilization of the antibacterial agents triclosan and triclocarban: effect of ionization and polymers. J. Incl. Phenom. Macrocycl. Chem. 52 (1–2), 109–117.

Mady, F.M., Ibrahim, M., Ragab, S., 2018. Cyclodextrin-based nanosponge for improvement of solubility and oral bioavailability of Ellagic acid. Pak. J. Pharm. Sci. 31 (5l), 2069–2076.

Mele, A., Castiglione, F., Malpezzi, L., Ganazzoli, F., Raffaini, G., Trotta, F., Rossi, B., Fontana, A., Giunchi, G., 2011. HR MAS NMR, powder XRD and Raman spectroscopy study of inclusion phenomena in βCD nanosponges. J. Incl. Phenom. Macrocycl. Chem. 69 (3–4), 403–409.

Mistri, H.N., Jangid, A.G., Sanyal, M., Shrivastav, P., 2007. Electrospray ionization LC–MS/MS validated method to quantify griseofulvin in human plasma and its application to bioequivalence study. J. Chromatogr. B 850 (1–2), 318–326.

Mognetti, B., Barberis, A., Marino, S., Berta, G., De Francia, S., Trotta, F., Cavalli, R., 2012. In vitro enhancement of anticancer activity of paclitaxel by a Cremophor free cyclodextrin-based nanosponge formulation. J. Incl. Phenom. Macrocycl. Chem. 74 (1–4), 201–210.

Moya-Ortega, M.D., Alvarez-Lorenzo, C., Concheiro, A., Loftsson, T., 2012. Cyclodextrin-based nanogels for pharmaceutical and biomedical applications. Int. J. Pharm. 428 (1–2), 152–163.

Muller, R.H., Keck, C.M., 2004. Challenges and solutions for the delivery of biotech drugs–a review of drug nanocrystal technology and lipid nanoparticles. J. Biotechnol. 113 (1–3), 151–170.

Nash R.A. 2002. Cyclodextrins. In: Handbook of pharmaceutical excipients, Academic Press, London, pp. 186–190.

Olteanu, A.A., Arama, C.-C., Bleotu, C., Lupuleasa, D., Monciu, C.M., 2015. Investigation of cyclodextrin based nanosponges complexes with angiotensin I converting enzyme inhibitors (Enalapril, captopril, cilazapril). Farmacia 63 (492–503), 1.

Parasuraman, S., Raveendran, R., Kesavan, R., 2010. Blood sample collection in small laboratory animals. J. Pharmacol. Pharmacotherap. 1 (2), 87.

Patel, A., Vavia, P.R., 2006. Effect of hydrophilic polymer on solubilization of fenofibrate by cyclodextrin complexation. J. Incl. Phenom. Macrocycl. Chem. 56 (1–2), 247–251.

Rao, M., Bajaj, A., Khole, I., Munjapara, G., Trotta, F., 2013. In vitro and in vivo evaluation of β-cyclodextrin-based nanosponges of telmisartan. J. Incl. Phenom. Macrocycl. Chem. 77 (1–4), 135–145.

Rao, M., Bhingole, R., 2015. Nanosponge-based pediatric-controlled release dry suspension of Gabapentin for reconstitution. Drug Dev. Industr. Pharm. 41(12), 2029–2036. doi:10.3109/03639045.2015.1044903.

Rao, M.R., Chaudhari, J., Trotta, F., Caldera, F., 2018. Investigation of cyclodextrin-based nanosponges for solubility and bioavailability enhancement of rilpivirine. AAPS PharmSciTech 19 (5), 2358–2369.

Rao, M.R., Shirsath, C., 2017. Enhancement of bioavailability of non-nucleoside reverse transciptase inhibitor using nanosponges. AAPS PharmSciTech 18 (5), 1728–1738.

Reverchon, E., Porta, G.D., Spada, A., Antonacci, A., 2004. Griseofulvin micronization and dissolution rate improvement by supercritical assisted atomization. J. Pharm. Pharmacol. 56 (11), 1379–1387.

Ribeiro, L., Loftsson, T., Ferreira, D., Veiga, F., 2003. Investigation and physicochemical characterization of vinpocetine-sulfobutyl ether β-cyclodextrin binary and ternary complexes. Chem. Pharm. Bull. 51 (8), 914–922.

Ritger, P.L., Peppas, N.A., 1987. A simple equation for description of solute release II. Fickian and anomalous release from swellable devices. J. Control. Release 5 (1), 37–42.

Salazar, S., Guerra, D., Yutronic, N., Jara, P., 2018. Removal of aromatic chlorinated pesticides from aqueous solution using β-cyclodextrin polymers decorated with Fe3O4 nanoparticles. Polymers 10 (9), 1038.

Sami, F., Philip, B., Pathak, K., 2010. Effect of auxiliary substances on complexation efficiency and intrinsic dissolution rate of gemfibrozil–β-CD complexes. AAPS PharmSciTech 11 (1), 27–35.

Sankalia, J.M., Sankalia, M.G., Mashru, R.C., 2008. Drug release and swelling kinetics of directly compressed glipizide sustained-release matrices: Establishment of level A IVIVC. J. Control. Release 129 (1), 49–58.

Shah, H.J., Subbaiah, G., Patel, D.M., Patel, C.N., 2009. In vitro–in vivo correlation of modified release dosage form of lamotrigine. Biopharm. Drug Dispos. 30 (9), 524–531.

Sharifmakhmalzadeh, B., Khodarahmpour, S., Salimi, A., 2014. Preparation and evaluation of the polymeric micellar formulation for oral delivery of griseofulvin. Int. J. Pharm. 4, 92–97.

Sharma, R., Walker, R., Pathak, K., 2011. Evaluation of the Kinetics and Mechanism of Drug Release from Econazole nitrate Nanosponge Loaded Carbapol Hydrogel, Vol. 45.

Silva, N., Moris, S., Díaz, M., Yutronic, N., Lang, E., Chornik, B., Kogan, M.J., Jara, P., 2016. Evidence of the disassembly of α-cyclodextrin-octylamine inclusion compounds conjugated to gold nanoparticles via thermal and photothermal effects. Molecules 21 (11), 1444.

Swaminathan, S., Vavia, P., Trotta, F., Torne, S., 2007. Formulation of betacyclodextrin based nanosponges of itraconazole. J. Incl. Phenom. Macrocycl. Chem. 57 (1–4), 89–94.

Swaminathan, S., Vavia, P.R., Trotta, F., Cavalli, R., Tumbiolo, S., Bertinetti, L., Coluccia, S., 2013. Structural evidence of differential forms of nanosponges of beta-cyclodextrin and its effect on solubilization of a model drug. J. Incl. Phenom. Macrocycl. Chem. 76 (1–2), 201–211.

Tejashri, G., Amrita, B., Darshana, J., 2013. Cyclodextrin based nanosponges for pharmaceutical use: a review. Acta pharmaceutica 63 (3), 335–358.

Torne, S., Darandale, S., Vavia, P., Trotta, F., Cavalli, R., 2013. Cyclodextrin-based nanosponges: effective nanocarrier for Tamoxifen delivery. Pharm. Dev. Technol. 18 (3), 619–625.

Trotta, F., Cavalli, R., Tumiatti, W., Zerbinati, O., Roggero, C., Vallero, R., 2008. Ultrasound-assisted synthesis of cyclodextrin-based nanosponges: U.S. Patent Application No. 11/630,403.

Trotta, F., Zanetti, M., Cavalli, R., 2012. Cyclodextrin-based nanosponges as drug carriers. Beilstein J. Org. Chem. 8 (1), 2091–2099.

Tsume, Y., Mudie, D.M., Langguth, P., Amidon, G.E., Amidon, G.L., 2014. The Biopharmaceutics Classification System: subclasses for in vivo predictive dissolution (IPD) methodology and IVIVC. Eur. J. Pharm. Sci. 57, 152–163.

Zainuddin, R., Zaheer, Z., Sangshetti, J.N., Momin, M., 2017. Enhancement of oral bioavailability of anti-HIV drug rilpivirine HCl through nanosponge formulation. Drug Dev. Ind. Pharm. 43 (12), 2076–2084.

Zidan, M.F., Ibrahim, H.M., Afouna, M.I., Ibrahim, E.A., 2018. In vitro and in vivo evaluation of cyclodextrin-based nanosponges for enhancing oral bioavailability of atorvastatin calcium. Drug Dev. Ind. Pharm. 44 (8), 1243–1253.

Zoppi, A., Quevedo, M.A., Longhi, M.R., 2008. Specific binding capacity of β-cyclodextrin with cis and trans enalapril: physicochemical characterization and structural studies by molecular modeling. Bioorg. Med. Chem. 16 (18), 8403–8412.